Journal of Southeast University (English Edition) Vol. 28, No. 1, pp. 58 – 63 Mar. 2012 ISSN 1003—7985

# Dynamic response of fixed-roof oil-storage tank structure under blast loading

Lu Shengzhuo Wang Wei

(College of Civil Engineering, University of Harbin Institute of Technology, HarBin 150090, China)

**Abstract:** In order to investigate the damage and deformation mechanism of large scale steel fixed-roof oil-storage tanks under the combustible gas explosion, a series of explosion experiments of scaled models are conducted. The 1∶25 scaled numerical models of oil-storage tanks with a capacity of 5 000 $m^3$ are also set up by ANSYS/LS-DYNA software, and their damage processes under the blast impact are numerically simulated. Both the experimental results and the numerical simulations show that the blast loading curve displays a pressure jump instantaneously at the moment of contact with the experimental models, and the overpressure peaks at the stagnation area of the outer surface on the blast side. The yield range first appears at the stagnation area and then propagates to the neighboring parts, and the irregular plastic hinge circle obviously appears around the deformation area, which results in the concaved buckling of the tank inner surface. During the whole process, the inner liquid not only impacts on the structures, but also absorbs and consumes part of the blast energy.

**Key words:** fixed-roof oil-storage tank; combustible gas explosion; numerical simulation and analysis; impact loading; dynamic strain

**doi:** 10.3969/j.issn.1003 – 7985.2012.01.011

With the fast development of the petrochemical industry, steel oil-storage tanks are now being widely used. However, the combustible and unsteady gas from the petroleum or petroleum products can burn easily, which can induce explosion accidents if mixed with air[1]. When an accident occurs, the air shock waves from the combustible gas explosion will severely damage the tanks, and even engender simultaneous explosions, which can in all probability destroy the entire oil depot or petroleum reserve base[2–3].

Based on a review of the literature, only a few studies have focused on the dynamic response of oil-storage tanks under external impact loads. Liu et al.[4–5] investigated the dynamic response of an underground steel cylindrical shell under the blast impact by the experiment of the steel cylindrical model. Pan et al.[6] simulated the damage of the thin-walled cylindrical tank by LS-DYNA. They investigated the damage under the explosion of a 50 $m^3$ tank filled with liquefied petroleum gas, but the blast load source was replaced by TNT according to the TNT equivalence method. However, there is little literature conducted on the behavior of a steel cylindrical tank subjected to the impact of combustible gas explosion. As the dynamic response of the large oil-storage tank structure is restricted by various influencing factors under the blast loading, it is difficult to accomplish prototype experiments. Inevitably, the results by only using the numerical simulation cannot reflect real situation.

This paper investigates the dynamic behaviors of scaled fixed-roof oil-storage tank models under impact loads of the combustible gas explosions by experiments. Meanwhile, the damage process of the 1∶25 scaled experimental model of an oil-storage tank with the capacity of 5 000 $m^3$ under the blast impact is also numerically simulated. The finite element (FE) numerical simulations and the experimental results are comparatively analyzed, and the characteristics of the gas blast load and the dynamic responses of a fixed-roof oil-storage tank under the blast impact are both investigated in this paper. The conclusions can provide a design basis for the study of large steel oil-storage tanks.

## 1 Experiment

### 1.1 Experimental models and test program

According to the structural plans of SINOPEC Engineering Incorporation and the Chinese national standard GB50341—2003, four experimental models are designed similar to the oil-storage tank prototypes with a capacity of 5 000 $m^3$, 10 000 $m^3$ and 20 000 $m^3$. Model 1 is designed according to the prototype with a capacity of 5 000 $m^3$ of full liquid level, and Model 2 is designed with a capacity of 5 000 $m^3$ of half of the liquid level. Model 3 and model 4 are designed with a capacity of 10 000 $m^3$ and 20 000 $m^3$, respectively.

Considering the limited space and test environments, the similarity ratio $\lambda$ is determined. In order to ensure that the stress, the strain and the deformation displacement are similar to the prototypes, special experimental

**Received** 2011-09-14.

**Biographies:** Lu Shengzhuo (1982—), male, graduate; Wang Wei (corresponding author), male, doctor, professor, wwang@hit.edu.cn.

**Foundation item:** The National Natural Science Foundation of China (No. 51078115).

**Citation:** Lu Shengzhuo, Wang Wei. Dynamic response of fixed-roof oil-storage tank structure under blast loading[J]. Journal of Southeast University (English Edition), 2012, 28(1): 58 – 63. [doi: 10.3969/j.issn.1003 – 7985.2012.01.011]

equipment is used, which makes the blast loading properties of the experiments similar to those of accidental explosions to satisfy the conditions of kinematic and dynamic similarities. Tab. 1 shows the geometrical dimension, the liquid level and other design parameters of the models. *H* and *h* represent the total height and the height of the oil-storage tank (body without fixed roof), respectively. Moreover, instead of oil, water is used to simulate the liquid pressure transfer. The inner liquid levels are also similar to their prototypes.

**Tab. 1** Design parameters of the experimental models

| Experimental model | Similarity $\lambda$ | Diameter/mm | $H$/mm | $h$/mm | Thickness $\delta$/mm | Liquid level $l$/mm |
|---|---|---|---|---|---|---|
| Model 1 | 25 | 800 | 800 | 712 | 1.0 | 600 |
| Model 2 | 25 | 800 | 800 | 712 | 1.0 | 300 |
| Model 3 | 38 | 790 | 504 | 418 | 1.0 | 390 |
| Model 4 | 38 | 974 | 650 | 513 | 1.0 | 480 |

### 1.2 Experimental procedure

The experiments are conducted in the gas blast and shocking (GBS) system, which includes four parts: the air and acetylene transmitting components, the ignition and control panel, the blast loading facility, and the anti-blast vessel. Before the tests begin, the end side is blocked by a plastic film so as to be enclosed. Then, air and acetylene are pumped into the facility according to a certain volumetric concentration. As the mixture is ignited, the gas explosion produces detonation waves instantaneously. The detonation waves spread along the blast loading facility, and they are injected into the anti-blast vessel. At the same time, the waves induce air shock waves impacting on the experimental models[7-8].

Pressure points *A*, *B*, *C* and *D* are located on the models' surfaces, which are used to measure the impact loads on the outer surfaces of the structures. Pressure point *E*, fixing on the inner surface of the models, is used to detect the liquid impact effects on the inner shell. Also, strain gauges are glued on the inner surface of each model. The arrangement detail of the pressure points is shown in Fig. 1.

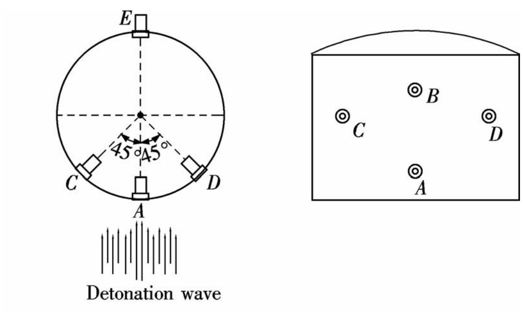


**Fig. 1** Schematic of pressure arrangement. (a) Vertical view; (b) Front elevation

## 2 Results and Discussion

The blast loading and the dynamic responses of the models are measured in each test, but it is impossible to list them all in this paper. In the following, the typical results of Model 1 and Model 2 are analyzed.

### 2.1 The overpressure history curves

The results of the blast loading and the liquid impact on selected regions of Model 1 are shown in Fig. 2. The curves of pressure points *A* and *C* display a typical dynamic change due to the gas blast.

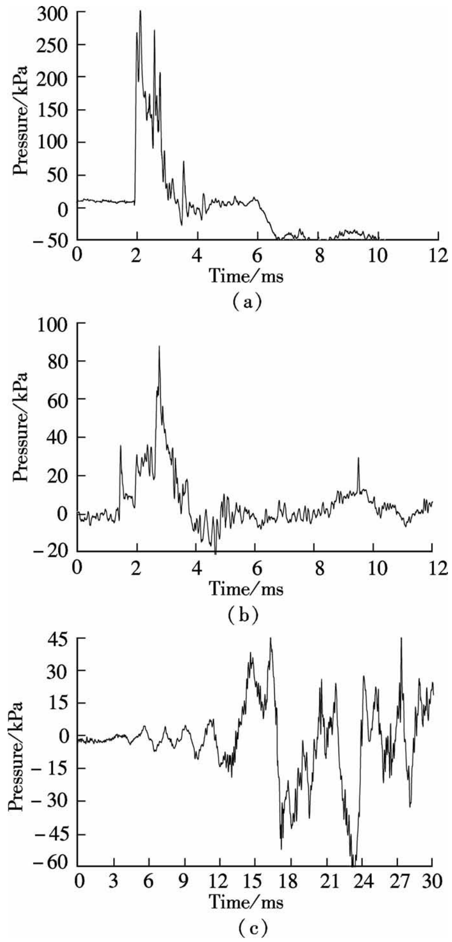


**Fig. 2** Overpressure history curves of Model 1. (a) Pressure point *A*; (b) Pressure point *C*; (c) Pressure point *E*

First, the overpressures increase instantaneously. After arriving at the peak value, they gradually descend to the negative pressure, and the downtrend fits to some exponential function. The positive pressure phase is less than 3 ms. Then, the oscillation occurs. In one test, the pressures are different according to the same blast loading. The frontal pressure point *A* reaches the maximum of peak overpressure, which is 161 to 282 kPa, while the peak value of pressure point *C*, located on the side surface, is 62 to 93 kPa, which is only one third of that of pressure point *A*. At the same time, pressure point *E* indicates that the inner liquid can transmit the compression wave to collide with the structure of the tank. The impact load transmitted by liquid collision has the same order of magnitude but a longer actuation duration than that of the blast wave.

### 2.2 The dynamic strain history curves

Fig. 3 presents the arrangement of dynamic strain gauges in experiments. As shown in Fig. 4, the changing process of dynamic strain is more complicate than that of the blast loading. In Fig. 4(a), the strain of Gauge 2 reaches a peak value of $1\ 382 \times 10^{-6}$ in 50 ms after the blast wave. Suddenly, it decreases nearly to zero and then starts another rise at once in a severe oscillation. Then, it ascends to the second peak, about $803 \times 10^{-6}$, and oscillates between $200 \times 10^{-6}$ and $600 \times 10^{-6}$. The strain history curve stops oscillating at $400 \times 10^{-6}$, and the residue strain appears on the model surface. The history curve of Gauge 5 shows that it ascends to the first peak value of $382 \times 10^{-6}$ and descends to the negative maximum. After that, the curve repeats the process of rise and fall and oscillates around zero. The strain history of Gauge 5 shows that that region of the tank shell experiences the alternative tension and compression under the blast loading and the impact of the inner liquid. The strain history of Gauge 6 and Gauge 5 are similar, which refers to the same alternative tension and compression on the rear surface of the tank. But the peak strains of Gauge 6 are less than those of Gauge 2 and Gauge 5.

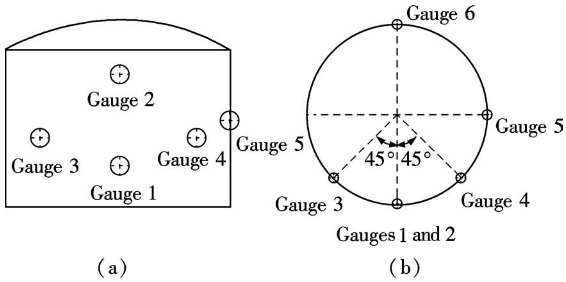


**Fig. 3** Arrangement of dynamic strain gauge. (a) Front elevation; (b) Vertical view

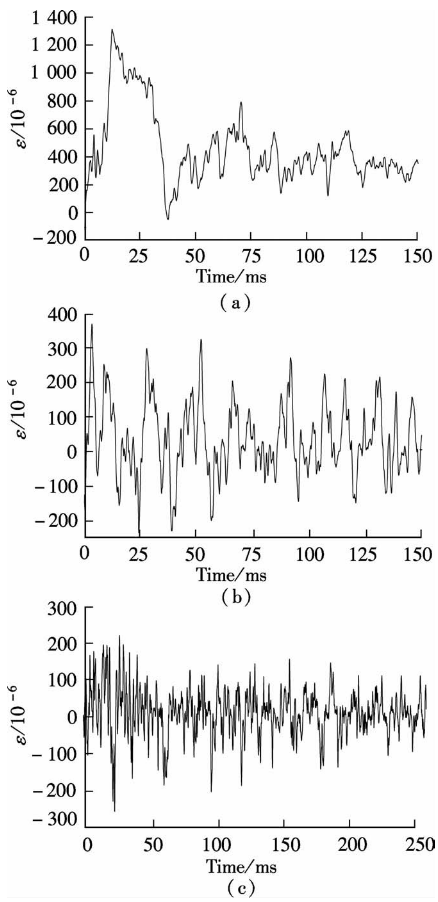


**Fig. 4** The strain history curves of Model 1. (a) Gauge 2; (b) Gauge 5; (c) Gauge 6

## 3 Comparative Analysis between Experimental Results and FE Numerical Simulations

Since the FE simulation method is an efficient way to study the dynamic response of structures under the blast load, the FE software is employed for numerical simulations in this paper. The nonlinear ANSYS/LS-DYNA finite element software plays an important role in making up the limitations and deficiencies of experiments. Therefore, the behaviors of the fixed-roof oil-storage tank scaled model under the combustible gaseous explosion are numerically simulated.

### 3.1 The FE model

In numerical simulations, the fluid structure interaction (FSI) method is used to calculate the blast wave and the inner liquid impact action with the model, respectively. Shell elements Shell163 are established to model the fixed-roof oil-storage tank model (about 43 000 elements). The material model of Q235 steel is chosen as the multilinear kinematic hardening model, *MAT_PLASTIC_KINEMATIC, which takes strain rate into account and is especially suitable for the steel in ANSYS/LS-DYNA. The initial yielding stress is 235 MPa; the elastic modulus is 206 GPa; the Poisson ratio is 0.3.

In respect that the reactant and the explosive products both follow the features of perfect gases, the perfect gas state equation, the $\gamma$-law equation, is defined to describe the dynamic change of gaseous explosive products. The reaction model of air and acetylene is built by the *MAT_HIGH_EXPLOSIVE_BURN and the *EOS_LINEAR_POLYNOMINAL state equations. Moreover, by ANSYS/LS-DYNA, the perfect gas state equation, the $\gamma$-law equation, does not complete until defining the parameters in the *EOS_LINEAR_POLYNOMIAL state equation. The $\gamma$-law equation is

$$P = \frac{E(\gamma - 1)}{V} \tag{1}$$

The air is modeled by the *MAT_NULL material model and the *EOS_LINEAR_POLYNOMINAL state equation. Solid elements Solid164 are used to model the air and the combustible gas. Tab. 2 lists the FE model parameters of the air and the combustible gas. Here $\rho$ is the density; $D$ is the detonation velocity; $P_{CJ}$ is the CJ pressure; and $E_0$ is the initial energy.

**Tab. 2** Parameters of finite element numerical simulation model

| Material | $\rho/(\mathrm{kg \cdot m^{-3}})$ | $D/(\mathrm{m \cdot s^{-2}})$ | $P_{CJ}$/GPa | $C_0$ | $C_1$ | $C_2$ | $C_3$ | $C_4$ | $C_5$ | $C_6$ | $E_0/(\mathrm{MJ \cdot m^{-3}})$ | $V_0$ |
|---|---|---|---|---|---|---|---|---|---|---|---|---|
| Combustible gas | 1.278 | 2 011 | 2.28 | 0 | 0 | 0 | 0 | 0.262 | 0.262 | 0 | 4.348 | 1.0 |
| Air | 1.293 | — | — | $-1.0\times10^5$ | 0 | 0 | 0 | 0 | 0 | 0 | 0.25 | 1.0 |

The damage performance of Model 1 and Model 2 under the blast impact is analyzed by the finite element method, and the deformation state by numerical simulations is much closer to that of the experimental results. The FE numerical simulations and the experimental results are comparatively analyzed, and the characteristics of the blast loading and the dynamic responses of the fixed-roof oil-storage tank under the blast impact are investigated in following sections.

### 3.2 Analysis of the gas blast loading

Fig. 5 shows the feature of the blast loading on Model 1 by FE numerical simulations. Compared with the overpressure history curves in Fig. 2, we can see that the numerical results is similar to the experimental results.

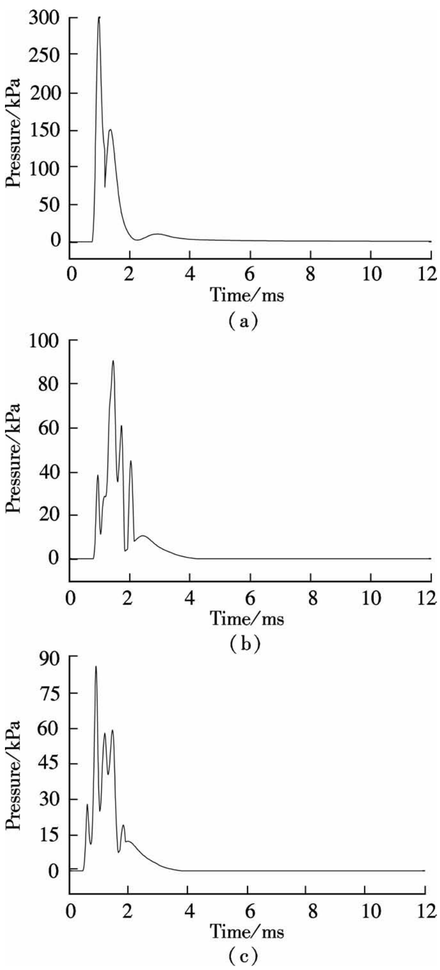


**Fig. 5** Overpressure history curves from numerical simulation results of Model 1. (a) Pressure $A$; (b) Pressure $C$; (c) Pressure $D$

Besides, the maximum peak values both appear on the stagnation area of the models. Tab. 3 lists the peak overpressure in experiments and FE numerical calculations.

The data in Tab. 3 illustrates that the blast loads decrease nonlinearly with the incident angle increasing, along the cylindrical shell's circumferential direction. On the one hand, a series of complicate shock waves are generated, because the reflected waves are interfered with by successive incident waves. On the other hand, the viscous friction dissipates the explosion energy in the process of flowing around the cylindrical surface, and the peak overpressure drops along the circumferential direction.

**Tab. 3** Peak overpressure from experimental results and numerical simulations

| Pressure point | Model 1 | | Model 2 | |
|---|---|---|---|---|
| | Experimental result /MPa | Numerical simulation /MPa | Experimental result /MPa | Numerical simulation /MPa |
| $A$ | 0.282 | 0.298 | 0.161 | 0.173 |
| $B$ | 0.144 | 0.151 | 0.085 | 0.091 |
| $C$ | 0.093 | 0.091 | 0.062 | 0.068 |
| $D$ | 0.089 | 0.087 | 0.078 | 0.077 |
| $E$ | 0.116 | 0.102 | 0.047 | 0.092 |

### 3.3 Characteristics of dynamic responses of fixed-roof oil-storage tank

Fig. 6 shows the dynamic strain history curves of Model 1 in numerical simulations. From the figures, it can be seen that the curves of the numerical calculations are identical to those of the experimental results, and so are their structural response times and peak values. Tab. 4 compares the peak values of the strain of Model 1 and Model 2 by the experimental results and the numerical simulations. Model 5 represents the same model as Model 1 and Model 2 without any liquid in the numerical simulation. The peak values of strain in the numerical simulations are close to those of the experimental results. The relative errors between the experimental results and the numerical simulations are 2.8% to 11.3%.

Combining the numerical simulation results with the experimental results, the damage process of Model 1, Model 2 and Model 5 can be described as follows: under the blast load, the yield range first appears at the

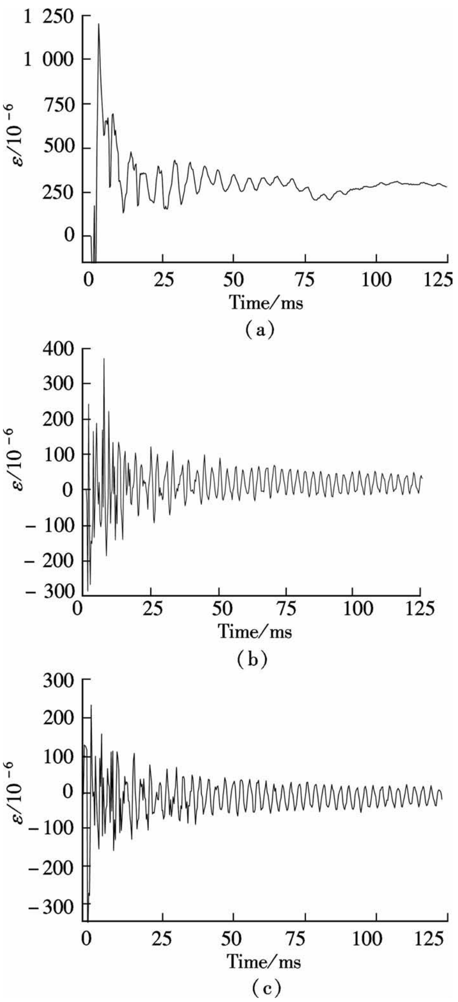


**Fig. 6** Dynamic strain history curves from numerical simulation results of Model 1

**Tab. 4** Peak values of strain of experimental results and numerical simulations $10^{-6}$

| Gauge | Model 1 | | Model 2 | | Model 5 |
|---|---|---|---|---|---|
| | Experimental results | Numerical simulation | Experimental results | Numerical simulation | Numerical simulation |
| 1 | 950 | 1 011 | −1 800 | −1 762 | −3 058 |
| 2 | 1 382 | 1 297 | −1 135 | −1 194 | −2 014 |
| 3 | 403 | 435 | −1 623 | −1 526 | −2 028 |
| 4 | 537 | 476 | −1 638 | −1 573 | −2 360 |
| 5 | 382 | 366 | 730 | 788 | −512 |
| 6 | 245 | 238 | −971 | −904 | −575 |

stagnation area on the top and middle parts of the tank body. Then, the plastic deformation extends to the neighboring area, and the concave deformation forms. With the continuous appearance of peak pressures on the other regions of the frontal surface, the bulking area expands and the displacement increases gradually. After the blast load abates, the deformation reaches the maximum displacement, and the area stops expanding. Then, the phenomenon of accelerated rebounds and oscillations appear on the concave deformation area. The oscillation stops at a new balance, and the residual deformation is formed ultimately. In the above procedure, the blast waves become weaker and weaker constantly, and the elastic strain energy and kinetic energy mutually transforms. Due to the weakened impact loads, the lateral and rear surfaces keep oscillating elastically all the time.

According to Tab. 4 and the numerical simulations, it is found that Model 5 (with no liquid) experiences more serious damage than the other two. The maximum deformation displacement of the frontal surface is 36 mm in Model 5. The deformation displacement of Model 1 is 11 mm, which is not so significant as that of Model 2, 15mm, in experiments and numerical simulations. Once the blast wave impacts on the structure instantaneously, the inner liquid is difficult to transform freely due to the effects of inertia. It initially behaves the elastic properties of the solid, and soon, it repeatedly changes its form with the vibration and transformation of the tank. The above vibration and friction of the liquid can absorb part of the blast energy. It can be summed up that the inner liquid both impacts and destroys the surface of the oil-storage tank, and absorbs some of the blast energy to reduce the deformation.

## 4 Conclusions

The blast load and the dynamic strain of the fixed roof oil-storage tank scaled models are obtained by impact experiments. Meanwhile, the FE code ANSYS/LS-DYNA is used to analyze the dynamic response of different oil-storage tank scaled models under the blast impact. From the comparisons between the experimental results and the numerical simulations, some conclusions can be drawn as follows:

1) The impact load from the gas explosion experiences an instantaneous pressure jump and a gradual reduction. The downtrend is fitted to some exponential function. The overpressures peak at the stagnation area of the outer surface on the blast side, and decrease along the circumferential direction on the cylindrical surface.

2) Due to the sudden impact effect, the yield range first appears at the stagnation area and then propagates to the neighboring area. Besides, the irregular plastic hinge circle obviously appears near that area in the process of deformation when the structure has resisted blast impacts. The area finally reaches a new balance after oscillation, while the other surfaces still keep oscillating elastically under the blast impact.

3) Under blast loading, the liquid inside impacts on the oil-storage tank inner surface; and it absorbs and consumes part of the blast energy as well.

## References

[1] Bjerketvedt D, Bakke J R, van Wingerden K. Gas explosion handbook [J]. *Journal of Hazardous Material*, 1997, **52**(1):50−72.

[2] Sari A, Whitney M, Sawruk W. Blast analysis and retrofit of structures in industrial facilities [C]//*Proceedings of the* 2009 *Structures Congress—Don't Mess with Structural Engineers*: *Expanding Our Role*. Austin, TX, USA, 2009:2075 − 2076.

[3] Baker D D. Advanced analysis topics for blast resistant buildings in petrochemical facilities[C]//*Proceedings of the* 2008 *Structures Congress—Structures Congress* 2008: *Crossing the Borders*. Vancouver, BC, Canada, 2008.

[4] Liu Xinyu, Ma Linjian, Ma Shuna. Model experiment on force characteristic of soil-embedded steel oil-tank under nuclear explosion [J]. *Journal of PLA University of Science and Technology*: *Natural Science Edition*, 2009, **10** (2):175 − 178. (in Chinese)

[5] Liu Xinyu, Qiu Xuguang, Zhang Chuan. Computation method of dynamic loads of underground steel cylindrical shell under nuclear explosion [J]. *Journal of PLA University of Science and Technology*: *Natural Science Edition*, 2006, **7**(4):360 − 364. (in Chinese)

[6] Pan Xuhai, Xu Jin, Jiang Juncheng, et al. Simulation analysis of dynamic response of thin-wall cylindrical tank to shock wave. [J]. *Journal of Chemical Industry and Engineering*, 2008, **59**(3):798 − 801. (in Chinese)

[7] Lu Shengzhuo, Wei Wang. Study of destruction mechanism of floating-roof oiltank under combustible gaseous explosion in a small scale experiment [J]. *Applied Mechanics and Materials*, 2012, **137**: 65 − 71.

[8] Lu Shengzhuo, Wang Wei, Zhang Boyi, et al. Experimental research on destruction mechanism of large-scale floating-roof oil tank under blast loading. [J]. *Explosion and Shock Waves*, 2011, **31**(2):158 − 164. (in Chinese)

# 爆炸冲击作用下拱顶式储油罐结构的动力响应

路胜卓　　王　伟

(哈尔滨工业大学土木工程学院,哈尔滨 150090)

**摘要:**为研究大型钢制拱顶式储油罐在可燃气体爆炸作用下的破坏和变形特征,对多个储油罐缩比模型进行爆炸实验. 并利用 ANSYS/LS-DYNA 软件,建立了缩比为 1∶25 的 5 000 $m^3$ 储油罐数值模型,对模型在爆炸冲击作用下的破坏过程进行数值模拟. 实验与数值结果表明:爆炸冲击波对储油罐缩比模型具有瞬间突跃增压的冲击特性,罐壁迎爆面驻点区域超压峰值最高;迎爆面中部驻点区首先屈服并带动相邻部分达到屈服状态,同时在变形区周围明显形成不规则的塑性铰环,导致罐壁产生内凹屈曲. 在此过程中,罐内液体既对罐壁产生一定的冲击作用,也能吸收和耗散部分爆炸能量.

**关键词:**拱顶式储油罐;可燃气体爆炸;数值模拟与分析;冲击荷载;动态应变

**中图分类号:**O382